Earth and Planetary Science Letters 417 (2015) 57–66

Contents lists available at ScienceDirect

Earth and Planetary Science Letters

www.elsevier.com/locate/epsl

Spin state transition and partitioning of iron: Effects on mantle dynamics

Kenny Vilella [a,*], Sang-Heon Shim [b], Cinzia G. Farnetani [a], James Badro [a,c]

[a] Institut de Physique du Globe de Paris, Sorbonne Paris Cité, 75005 Paris, France
[b] School of Earth and Space Exploration, Arizona State University, 781 S. Terrace Road, Tempe, AZ 85281, USA
[c] École Polytechnique Fédérale de Lausanne, CH-1015 Lausanne, Switzerland

ARTICLE INFO

Article history:
Received 23 July 2014
Received in revised form 17 December 2014
Accepted 10 February 2015
Available online xxxx
Editor: J. Brodholt

Keywords:
spin state transition
Earth's lower mantle
Fe partitioning
convection
geodynamics

ABSTRACT

Experimental studies at pressure and temperature conditions of the Earth's lower mantle have shown that iron in ferropericlase (Fp) and in Mg-silicate perovskite (Pv) undergoes a spin state transition. This electronic transition changes elastic and transport properties of lower mantle minerals and can play an important role in mantle convection. Here we focus on the geodynamic effect of the spin-induced density modifications caused by the volume collapse of Fp and by the variation of Fe partitioning (K^{Pv-Fp}) between Fp and Pv. Since K^{Pv-Fp} behavior strongly depends on alumina content, we explore two end-member compositions, one Al-bearing (with 4.7 wt% Al_2O_3 in Pv) and the other Al-free. We use the theoretical model by Sturhahn et al. (2005) to calculate the spin configuration of Fp over a range of pressure–temperature conditions, and use experimental results to model Fe partitioning. We then apply the Mie–Grüneisen–Debye equation of state to obtain the density of the mineral assemblages. The calculated amplitude of the density change across the spin state transition is less than 1%, consistent with experiments by Mao et al. (2011); our density profiles differ from PREM by less than 1.5%. The spin-induced density variations are included in a three dimensional convection code (Stag3D) for a compressible mantle. We find small temperature differences between models with and without spin state transitions, since over billions of years the relative temperature difference is less than 50 K. However the relative RMS vertical velocity difference is up to 15% for an Al-free system, but only less than 6% for an Al-bearing system.

1. Introduction

The widely accepted pyrolitic compositions consist of approximately 18 vol% ferropericlase $(Mg,Fe)O$ (hereafter called Fp), 75 vol% Mg-silicate perovskite $(Mg,Fe)(Al,Si)O_3$ (hereafter called Pv), and 7 vol% Ca-silicate perovskite $CaSiO_3$ (hereafter called CaPv) (Ringwood, 1982; Irifune, 1994; Irifune et al., 2010). Even if the uncertainties in the composition of the lower mantle are considered, current experiments at high pressure and temperature, coupled with equations of state (Jackson, 1998; Ricolleau et al., 2009; Murakami et al., 2012) cannot fully explain density and seismic velocities inferred by seismic models such as PREM (Dziewonski and Anderson, 1981). The disagreement reveals the large uncertainties that still affect composition, temperature, and physical properties in the lower mantle.

Fyfe (1960) suggested that the electronic structure of Fe^{2+} in the octahedral coordination can change at high pressure. For example, the 3*d* orbitals of Fe^{2+} in Fp, which is surrounded by six oxygen atoms, split in two different groups with different energies: three orbitals (t_{2g}) with a lower energy and two orbitals (e_{2g}) with a higher energy (see Li et al., 2004, Fig. 4). Following Hund's rule, at ambient condition, the stable state has two unpaired electron in two t_{2g} orbitals, two unpaired electrons in two e_{2g} orbitals, and two paired electrons in a t_{2g} orbital. This configuration is the high spin (HS) state. With compression, the splitting of the two energy levels can increase and at some point the energy gap becomes large enough to stabilize the state with six paired electrons in the t_{2g} orbitals. This configuration is the low spin (LS) state. Sherman (1988) and Burns (1993), with a crystal field theory, as well as Cohen et al. (1997), with a band theory, predicted the occurrence of such change in spin state at the pressure–temperature conditions of the Earth's lower mantle. Badro et al. (2003) found a spin state transition in Fp at a pressure range ~60–70 GPa and at ambient temperature. At higher temperatures, theoretical models (Sturhahn et al., 2005; Tsuchiya et al., 2006) predicted that the

* Corresponding author.
E-mail address: vilella@ipgp.fr (K. Vilella).

http://dx.doi.org/10.1016/j.epsl.2015.02.009
0012-821X/

spin state transition should occur at higher pressure and over a broad range of pressure, as confirmed by Lin et al. (2007a). Iron spin state transitions occur also in Pv (Badro et al., 2004; Jackson et al., 2005), but it is more complex because of two different crystallographic sites, an octahedral and a dodecahedral, and two different oxidation state of iron, Fe^{2+} and Fe^{3+} (see Lin et al., 2013; Badro, 2014, and reference therein).

Spin state transitions alter the elastic and transport properties (Jackson et al., 2006; Lin et al., 2006, 2007b, 2013; Crowhurst et al., 2008; Goncharov et al., 2008, 2009; Antonangeli et al., 2011; Ammann et al., 2011) thereby affecting mantle dynamics. Moreover the lower mantle density is modified by the volume collapse due to the lower volume of Fe^{2+} in LS state, and by the spin state induced modification of Fe partitioning between Fp and Pv. Bower et al. (2009) and Shahnas et al. (2011) calculated the property changes induced by the Fe^{2+} spin state transition in Fp, and conducted numerical simulations to quantify the effect on mantle dynamics. Both studies found increased mantle temperature and enhanced flow velocity. However, Bower et al. (2009) assumed a pure Fp composition and Shahnas et al. (2011) neglected Fe partitioning, so that both studies use a simplified lower mantle composition.

Here we use a theoretical model (Sturhahn et al., 2005) coupled to an equation of state (Jackson and Rigden, 1996) to build a density model including the Fe^{2+} spin state transition in Fp. The dominant chemical components (e.g., FeO, MgO, $MgSiO_3$, Fe_2O_3, Al_2O_3, etc.) are included in order to provide realistic thermodynamic properties of the mineral assemblages (Fp, Pv, and CaPv). We apply an equation of state to these minerals to obtain their density as a function of pressure and temperature. This approach enables us to explore different compositions and to calculate the corresponding density profile.

A new aspect of our work is to consider the spin state induced Fe partitioning between Pv and Fp ($K^{\mathrm{Pv-Fp}}$). Recent experiments have shown different behaviors of $K^{\mathrm{Pv-Fp}}$ for an olivine composition (Kobayashi et al., 2005; Sinmyo et al., 2008; Auzende et al., 2008; Sakai et al., 2009) and pyrolitic compositions (Irifune, 1994; Kesson et al., 1998; Wood, 2000; Murakami et al., 2005; Irifune et al., 2010; Sinmyo and Hirose, 2013). Therefore we study two end-member compositions, an Al-bearing and an Al-free pyrolite, with their corresponding Fe partitioning. We assume that in the Al-free system Fe partitioning follows the same behavior as in the olivine composition. The calculated density profile in the lower mantle fits PREM density (Dziewonski and Anderson, 1981) within 1.5%, using Brown and Shankland (1981) geotherm, and it is consistent with high temperature experiments (Mao et al., 2011). The density models are then included in the convection code Stag3D (Tackley, 1996) to quantify the long term impact of the Fe spin state transition on mantle convection.

2. Density models

This paragraph presents how we calculate: (a) the average spin sate of Fe^{2+} in Fp, (b) the iron content of Fp and Pv, considering Fe partitioning, and (c) the density variations induced by the spin state transition for two end-member lower mantle compositions.

2.1. Average spin state of iron in ferropericlase

Following Sturhahn et al. (2005) we calculate the average Fe^{2+} spin configuration in Fp by minimizing the Helmholtz free energy: $F = U - TS$. Note that by considering the Helmholtz free energy, rather than the Gibbs free energy, Sturhahn et al. (2005) implicitly neglect work variations during the spin state transition. Only LS state Fe^{2+} ions interact with each other, thus the internal energy is

$$U = -N J_{\mathrm{LS}} \eta_{\mathrm{LS}}^2 + N(\eta_{\mathrm{LS}} E_{\mathrm{LS}} + \eta_{\mathrm{HS}} E_{\mathrm{HS}}), \tag{1}$$

where N is the number of Fe^{2+} in Fp, E_{LS} and E_{HS} are the energy levels of LS state and HS state, respectively, J_{LS} is the coupling LS state-LS state, η_{LS} and η_{HS} the fractions of Fe^{2+} in LS state and HS state, respectively, with $\eta_{\mathrm{LS}} + \eta_{\mathrm{HS}} = 1$. The entropy of the crystal can be written as

$$S = -k_B N \left[\eta_{\mathrm{LS}} \ln\left(\frac{\eta_{\mathrm{LS}}}{g_{\mathrm{LS}}}\right) + \eta_{\mathrm{HS}} \ln\left(\frac{\eta_{\mathrm{HS}}}{g_{HS}}\right) \right], \tag{2}$$

where k_B is the Boltzmann constant, g_{LS} and g_{HS} are the energy degeneracies of the electronic configuration. The free energy is then:

$$F = N\Big\{ - J_{\mathrm{LS}} \eta_{\mathrm{LS}}^2 + \eta_{\mathrm{HS}} E_{\mathrm{HS}} + \eta_{\mathrm{LS}} E_{\mathrm{LS}} + k_B T \left[\eta_{\mathrm{LS}} \ln\left(\frac{\eta_{\mathrm{LS}}}{g_{\mathrm{LS}}}\right) + \eta_{\mathrm{HS}} \ln\left(\frac{\eta_{\mathrm{HS}}}{g_{\mathrm{HS}}}\right) \right] \Big\}. \tag{3}$$

To find the equilibrium state at a given condition we solve

$$\frac{\partial F}{\partial \eta_{\mathrm{LS}}} = 0. \tag{4}$$

By using the normalized equation, we express Eq. (4) as:

$$0 = \eta_{\mathrm{LS}} \left[1 + \frac{g_{\mathrm{HS}}}{g_{\mathrm{LS}}} \exp(-2\beta J_{\mathrm{LS}} \eta_{\mathrm{LS}}) \exp(\beta(E_{\mathrm{LS}} - E_{\mathrm{HS}})) \right] - 1, \tag{5}$$

with $\beta = k_B T$. J_{LS} depends on the iron content and volume, E_{LS} and E_{HS} depend on volume (Sturhahn et al., 2005), the remaining parameters are assumed to be constant. The solution of Eq. (5) provides the fraction of LS state as a function of iron content, volume, and temperature. For further details on the parameters values please refer to Sturhahn et al. (2005).

The next step is to convert volume to pressure using the Mie–Grüneisen–Debye equation of state (Jackson and Rigden, 1996) and the parameters listed in Tables 1 and 2. At ambient temperature we use the third order Birch–Murnaghan equation of state:

$$P = \frac{3K_{T0}}{2} \left[\left(\frac{V_0}{V}\right)^{7/3} - \left(\frac{V_0}{V}\right)^{5/3} \right] \left\{ 1 - \frac{3}{4}(4 - K'_{T0}) \left[\left(\frac{V_0}{V}\right)^{2/3} - 1 \right] \right\} + \Delta P_{th}, \tag{6}$$

while the effect of temperature is added via a thermal pressure:

$$\Delta P_{th} = \frac{\gamma(V)}{V} [E_{th}(V, T) - E_{th}(V, T_0)], \tag{7}$$

where the subscript zero indicates ambient conditions for volume V_0, temperature T_0, isothermal bulk modulus K_{T0} and its pressure derivative K'_{T0}. The Grüneisen parameter depends on volume:

$$\gamma(V) = \gamma_0 \left(\frac{V}{V_0}\right)^q, \tag{8}$$

where q is assumed to be a constant. The vibrational energy is calculated from the Debye model,

$$E_{th} = \frac{9nRT^4}{\theta^3} \int_0^{\theta/T} \frac{x^3}{e^x - 1} dx, \tag{9}$$

n is the number of atoms per formula unit, R is the gas constant, and θ is the Debye temperature:

$$\theta = \theta_0 \exp\left(\frac{\gamma_0 - \gamma(V)}{q}\right). \tag{10}$$

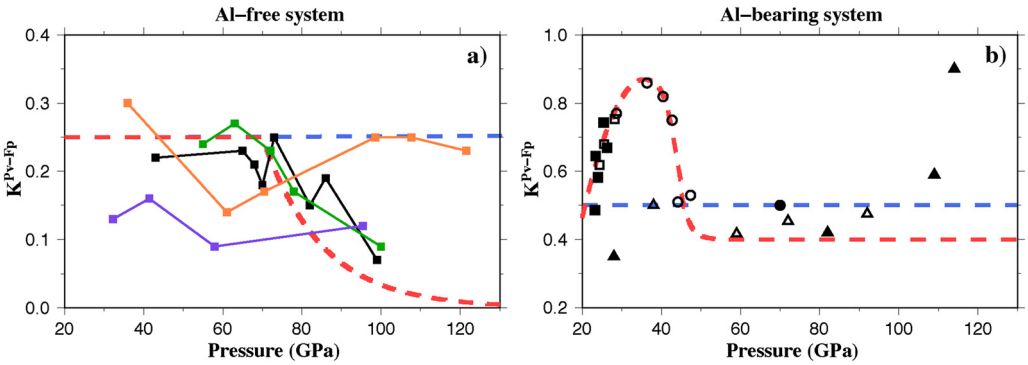

Fig. 1. Fe partitioning between Pv and Fp versus pressure. (a) For the Al-free system the experimental results (solid lines) are from: Kobayashi et al. (2005) (purple); Sinmyo et al. (2008) (orange); Auzende et al. (2008) (green); Sakai et al. (2009) (black). (b) For the Al-bearing system data by: Irifune et al. (2010) (open circles); Irifune (1994) (open squares); Wood (2000) (squares); Kesson et al. (1998) (circles); Murakami et al. (2005) (open triangles); Sinmyo and Hirose (2013) (triangles). In both panels the blue dashed line represents the constant partitioning used in the Reference-models without spin state transition, whereas the red dashed line represents the variable K^{Pv-Fp} used in our models with spin state transition (see text). (For interpretation of the references to color in this figure legend, the reader is referred to the web version of this article.)

Experimental results at ambient temperature show that K_{T0} for FeO could change with the spin state, however the pressure range of the LS state is too small to determine K_{T0} precisely (see Lin et al., 2013, for more details). At higher temperature, Mao et al. (2011) found a K_{T0} difference within the error bars. The change of K_{T0} for FeO due to spin state transition seems to have a minor effect on the lower mantle density, therefore we use the same value for both spin states. This set of equations enables us to calculate the average spin state as a function of iron content, temperature and pressure.

2.2. Iron content in ferropericlase and perovskite

Fe partitioning is measured with the Fe–Mg exchange coefficient between Pv and Fp,

$$K^{Pv-Fp} = \frac{\left(\frac{Fe}{Mg}\right)_{Pv}}{\left(\frac{Fe}{Mg}\right)_{Fp}} = \frac{\frac{1}{x_{Fp}} - 1}{\frac{1}{x_{Pv}} - 1}, \tag{11}$$

where x_{Pv} and x_{Fp} are the molar iron concentration in Pv and Fp, respectively.

Experimental studies have shown that Fe partitioning depends strongly on Al content, perhaps because of the coupled substitution of Al and Fe^{3+} in Pv and absence of such substitution for Fp (Navrotsky, 1999). For the Al-free system, the solid lines in Fig. 1a highlight two different behaviors: Kobayashi et al. (2005) and Sinmyo et al. (2008) found an almost constant partitioning with pressure, whereas Auzende et al. (2008) and Sakai et al. (2009) showed that Fe partitioning decreases dramatically at ~70 GPa, the pressure at which the spin state transition occurs in Fp. For the Al-bearing system, Fig. 1b shows the main experimental data as compiled by Irifune et al. (2010). A sharp increase of the partitioning at ~25 GPa (Irifune, 1994; Wood, 2000) is followed by a sharp decrease at ~40 GPa. At higher pressure the results are conflicting: Kesson et al. (1998) and Murakami et al. (2005) measured a constant partitioning, while Sinmyo and Hirose (2013) found an increase of Fe partitioning above 90 GPa.

Given the striking difference between the Al-free (Fig. 1a) and the Al-bearing (Fig. 1b) cases, we build two end-member models for lower mantle composition. Our first composition, called Al-free, has a classical lower mantle mineral volume proportion: 75% Pv, 18% Fp and 7% CaPv, with 8 wt% FeO in the bulk composition. All iron is assumed to be Fe^{2+}. Our second composition, called Al-bearing, differs from the previous one by the addition of 4.7 wt% Al_2O_3 and by assuming that 60% of iron in Pv is Fe^{3+}, the remaining is Fe^{2+}. Ferrous iron enters into Pv as $FeSiO_3$, ferric iron enters into Pv as $FeAlO_3$. If there is an excess of Fe^{3+}, Fe_2O_3 enters into Pv, whereas if there is an excess of Al, Al_2O_3 enters into Pv.

Table 1
Isothermal bulk modulus (K_{T0}) and volume (V_0) at ambient conditions for several compounds.

Compounds	K_{T0} (GPa)	V_0 (cm^3/mol)
MgO	160[a]	11.25[a]
FeO (LS)	150[b]	10.82[b]
FeO (HS)	150	12.18[b]
$MgSiO_3$	261[c]	24.43[c]
$0.85MgSiO_3$–$0.15FeSiO_3$	259 [c]	24.58[c]
$0.915MgSiO_3$–$0.085Fe_2O_3$	237[d]	24.95[d]
$0.90MgSiO_3$–$0.10FeAlO_3$	262[e]	24.80[e]
$0.90MgSiO_3$–$0.10Al_2O_3$	244[e]	24.66[e]
$CaSiO_3$	236[f]	27.45[f]

[a] Speziale et al. (2001).
[b] Fei et al. (2007).
[c] Lundin et al. (2008).
[d] Catalli et al. (2010).
[e] Catalli et al. (2011).
[f] Shim et al. (2000b).

These compositions are used in the models that include the spin state transition and a variable partitioning coefficient, as shown in Fig. 1 (red dashed lines), as well as in the corresponding reference models (called Reference Al-free and Reference Al-bearing), which are calculated without spin state transition and with a constant partitioning coefficient, as shown in Fig. 1 (blue dashed lines). The underlying assumption is that the change of partitioning is caused by the spin state transition. Badro et al. (2005) provide a thermodynamic argument for the Al-free system, and find that

$$K^{Pv-Fp} = K_0 \exp\left(-\frac{\Delta V (P - P_{tr})}{RT}\right), \tag{12}$$

where $\Delta V = 1.36$ cm^3/mol is the FeO volume difference between HS and LS states (Fei et al., 2007) and P_{tr} is the pressure of the spin state transition. The red dashed line in Fig. 1a is calculated using Eq. (12), which is in agreement with experimental results by Auzende et al. (2008) and by Sakai et al. (2009). For the Al-bearing system, we use a fit of experimental results by Irifune et al. (2010).

2.3. Density as a function of temperature and pressure

We calculate the density of each mineral using the average spin configuration and the Mie–Grüneisen–Debye equation of state detailed in Eq. (6) (standard values are listed in Tables 1 and 2). The composition of each mineral species changes with pressure and

Table 2
Equation of state parameters for lower mantle minerals: Perovskite (Pv), Ferropericlase (Fp) and Ca-Perovskite (CaPv).

Parameter	Pv	Fp	CaPv
K'_{T0}	3.7[a]	4[b]	3.9[c]
θ_0 (K)	1100[a]	673[b]	1000[c]
γ_0	1.4[a]	1.41[b]	1.92[c]
q	1.4[a]	1.3[b]	0.6[c]

[a] Fiquet et al. (2000).
[b] Jackson and Niesler (1982).
[c] Shim et al. (2000a).

temperature because of variations in Fe partitioning. The initial volume and bulk modulus (V_0 and K_{T0}) are obtained by linear interpolation between the Mg- and Fe-end-members. We then calculate the density of the rock as the weighted average of constituent mineral densities.

The relative density difference ($\Delta\rho = 100(\rho_{\text{Spin}} - \rho_{\text{Ref}})/\rho_{\text{Spin}}$) between the model with spin state transition and variable $K^{\text{Pv–Fp}}$ and the corresponding reference model is shown for Al free (Fig. 2a) and Al bearing (Fig. 2b) compositions. As found by theoretical and experimental studies, the spin state transition is sharp at low temperature and broad at high temperature. At $1200 < T < 1800$ K, our transition is sharper than experimental results (Komabayashi et al., 2010; Mao et al., 2011), but the difference vanishes at higher temperatures ($T > 2000$ K) appropriate to the lower mantle. The amplitude of the density change is ~0.8% for Al-free system and only ~0.5% for Al-bearing system, this difference is due to the Fe partitioning. In Fig. 2b the peak of $\Delta\rho$ at 35 GPa is due to Fe partitioning and clearly reflects the $K^{\text{Pv–Fp}}$ trend shown is Fig. 1b. Finally, we note that the calculated density changes are comparable with those found in experimental results, although a slight mismatch still exists. For example, at $T = 2000$ K we find the same density change as Mao et al. (2011), but our transition occurs at a pressure 10 GPa lower. This seems acceptable, given that a similar mismatch is observed between experimental studies (for a review see Lin and Tsuchiya, 2008). At a given pressure, the density change varies with temperature, so the temperature derivative of density is affected by the spin state transition. Therefore, the thermal expansivity, defined as $\alpha = (-1/\rho)(\partial\rho/\partial T)_p$, is also affected by the spin state transition. At lower mantle temperatures, α is locally increased up to ~40%. We also note that the mismatch between our density profile and PREM density, using Brown and Shankland (1981) geotherm, is less than 0.6% for reference models. Furthermore we conducted a number of simulations (not shown here) to gauge the effect of uncertainties in experimental results and found that they induce only small variations (less than 0.1%) in relative density differences, suggesting that our results are robust.

3. Mantle convection model

We include the calculated lower mantle density in a three dimensional geodynamic model. The code Stag3D (Tackley, 1996) in cartesian geometry solves the non-dimensional equations governing mantle convection, assuming the truncated anelastic approximation. The equations are: conservation of mass

$$\nabla \bullet (\bar{\rho}\underline{v}) = 0, \tag{13}$$

conservation of momentum

$$\nabla \bullet \underline{\underline{\sigma}} - \nabla p = Ra\bar{\rho}\bar{\alpha}T'\hat{z}, \tag{14}$$

conservation of energy

$$\bar{\rho}C_p\frac{DT}{Dt} = -Di_s\bar{\alpha}\bar{\rho}T'v_z + \nabla \bullet (\bar{k}\nabla T) + \bar{\rho}H + \frac{Di_s}{Ra}\underline{\underline{\sigma}} : \underline{\underline{\dot{\epsilon}}}. \tag{15}$$

$\bar{k}$ is the depth-dependent thermal conductivity, $\bar{\alpha}$ the depth-dependent thermal expansivity and $\bar{\rho}$ the depth-dependent density. T is temperature, $T' = T - T_{ref}$ the temperature anomaly with respect to the adiabatic temperature T_{ref}, p the dynamic pressure, $\underline{v}$ the velocity vector, H the internal heating rate, C_p the specific heat capacity, $\underline{\underline{\sigma}}$ the deviatoric stress tensor, $\underline{\underline{\dot{\epsilon}}}$ the strain rate tensor, $\hat{z}$ is a unit vector in the vertical direction. The truncated anelastic approximation neglects the variations of temperature due to the dynamic pressure, therefore we use the dynamic pressure rather than the total pressure. The two non-dimensional numbers are the surface dissipation number $Di_s = \alpha_s g D/C_p$ and the Rayleigh number $Ra = \rho g \alpha \Delta T D^3/\eta\kappa$ (see Table 3). To include our lower mantle density models (ρ_{model}) we must modify the equation of conservation of momentum, since the thermal expansivity depends on depth and spin state transition (i.e., on temperature). We modify the equation of conservation of momentum as follows

$$\nabla \bullet \underline{\underline{\sigma}} - \nabla p = Ra\frac{\Delta\rho_{model}}{\Delta\rho_{th}}\hat{z}, \tag{16}$$

where $\Delta\rho_{th} = \alpha\Delta T$ and $\Delta\rho_{model} = \rho_{model}(T_{ref}, p) - \rho_{model}(T, p)$. With this formulation the thermal expansivity does not appear explicitly. We approximate mantle viscosity via the following equation,

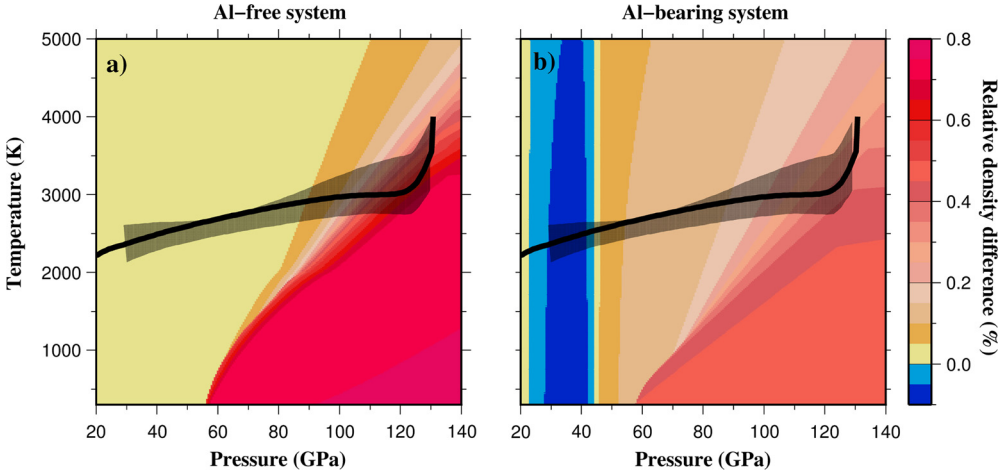

Fig. 2. Relative density difference (%) between the model with spin state transition and the reference model (without spin state transition), as a function of pressure and temperature, for (a) Al-free, and (b) Al-bearing compositions. The geotherm (black line) is from our numerical simulations, and the dotted area corresponds to the range of possible lower mantle temperatures by Deschamps and Trampert (2004), inferred from seismic models combined with experimental mineralogy data.

Table 3
Mantle parameters used in the numerical simulations.

Symbol	Parameter	Value	Non-dimensional value
Ra_0[a]	Surface Rayleigh number	10^7	N/A
Di_s[b]	Surface dissipation number	1.18	N/A
ρ_0	Surface density	3300 kg/m^3	1.0
g	Gravity	9.81 m/s^2	1.0
α_0	Surface expansivity	5×10^{-5} K^{-1}	1.0
ΔT	Superadiabatic temperature scale	2500 K	1.0
d	Mantle thickness	2890 km	1.0
κ_0	Surface thermal diffusivity	7×10^{-7} m^2/s	1.0
$C_{P,0}$	Surface heat capacity	1200 J/(kg K)	1.0
η_0	Reference viscosity	1.4×10^{22} Pa s	1.0
H	Internal heating rate	7.38×10^{-12} W/kg	15.5[c]
$\Delta\rho_{410}$	Density change at 410 km	198 kg/m^3	0.06
$\Delta\rho_{660}$	Density change at 660 km	462 kg/m^3	0.14
γ_{660}	Clapeyron slope at 410 km	−2.5 MPa/K	−0.066
γ_{660}	Clapeyron slope at 660 km	2.5 MPa/K	0.066

[a] $Ra_0 = \rho g \alpha \Delta T D^3/\eta\kappa$.
[b] $Di_s = \alpha_s g D/C_p$.
[c] Corrected for Cartesian geometry, see Tackley (1996) for further details.

$$\eta(T,d) = \eta_0 \exp(d\Delta\eta_d) \exp\left(\frac{13.8}{T+0.88}\right), \quad (17)$$

providing a four orders of magnitude variation with temperature and a tenfold increase from the surface to the core mantle boundary (CMB), for $\Delta\eta_d = 2.3$. At 660 km depth the viscosity increases by a factor 30 due to the phase transition. Numerical values of the Clapeyron slope and of the density change induced by the phase transitions at 660 km and 410 km depth are given in Table 3.

The modeled domain is divided in 1024 × 1024 × 128 elements, providing a spatial resolution of ∼22.6 km. The boundary conditions at top and bottom are free slip velocity and constant temperature (300 K and 4000 K, respectively), the side boundaries are periodic. The temperature field at equilibrium (i.e., after the equivalent of 15 Ga) is used as initial condition for the different numerical simulations. The four models are run for further 20 Ga and we avoid any influence of the initial condition by conducting time averages only over the last 7 Ga.

4. Results

Fig. 3 shows snapshots of the anomaly of potential temperature for the Al-bearing case and its corresponding reference case. Convection in both snapshots seems to be identical. Some cold downwellings are stopped at 660 km depth and create avalanches that reach the lower mantle (Fig. 4). Hot upwellings are also stopped at 660 km depth and form secondary plumes that reach the surface (Fig. 4).

The temperature field is averaged horizontally and temporally in order to calculate the relative temperature difference between models with and without spin state transition. The temperature difference (Fig. 5a) is almost constant in the whole mantle and varies sharply close to the surface and to the CMB. For the Al-bearing composition, the temperature increases by ∼0.6%, equivalent to a ∼20 K difference at ∼2500 km depth. The temporally averaged surface heat loss for the reference case is 42.7 TW, in the range of value inferred by Jaupart et al. (2007), and increases

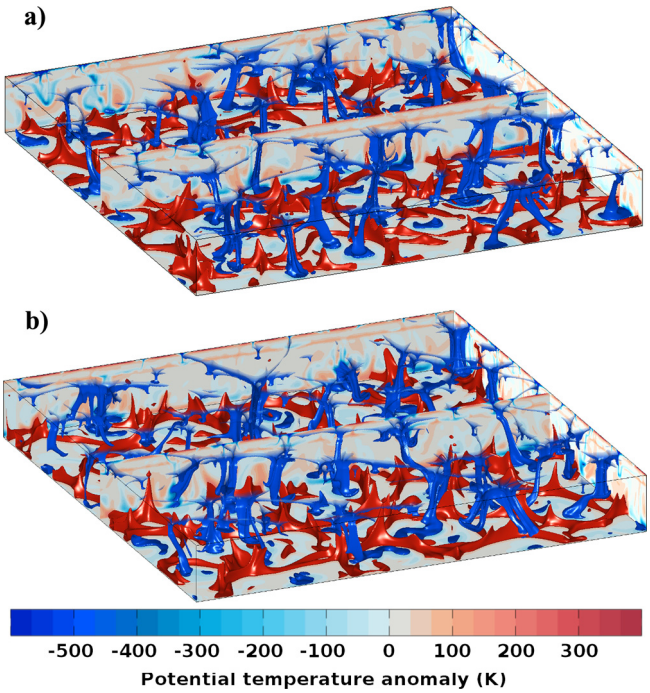

Fig. 3. Potential temperature anomaly ($T-T_m$, where T_m is the average temperature) for the Al-bearing case with the spin state transition (a) and without (b), the two isosurfaces (−450 K and 200 K) highlight downwellings and upwellings. For graphical reasons the cold isosurface (blue) is transparent at shallow depths and the temperature scale is truncated. (For interpretation of the references to color in this figure legend, the reader is referred to the web version of this article.)

to 43.2 TW with the spin state transition. Therefore the spin state transition slightly increases the efficiency of heat transfer. For the Al-free composition, the effects are similar but more significant with a temperature increase of ∼1.6%, equivalent to a ∼50 K difference at ∼2500 km depth. The temporally averaged surface heat loss for the reference case is 42.7 TW and 43.8 TW with the spin state transition, this ∼2.5% difference is much smaller than the uncertainty for the Earth (the range of plausible values by (Jaupart et al., 2007) is 43–49 TW). Since the temperature profile is close in both models, the corresponding relative density difference (Fig. 5b) reflects the density change due to the spin state transition found in Fig. 2. In the Al-free case the relative density difference increases at ∼100 GPa and deeper, but decreases in the lowermost ∼150 km ($125 < P < 135$ GPa) because the sharp temperature rise in the thermal boundary layer reduces the extent of LS state (as shown by the geotherm in Fig. 2). In the Al-bearing case the relative density increases at ∼40 GPa, is almost constant to ∼100 GPa and then increases to the CMB.

Fig. 4 shows a slice of the temperature field and the density change induced by the spin state transition. In plumes the LS to HS transition occurs at greater depth, so that the surrounding mantle is in LS state while the plume center is in HS state. This lateral density difference increases plume buoyancy and should enhance the upwelling velocity. In slabs the HS to LS transition occurs at shallower depth, thus the surrounding mantle is in HS state while the slab center is in LS state. The increased lateral density difference should enhance the downwelling velocity. We first study the RMS vertical flow velocity by separating upwelling and downwelling material with a criterion solely based on the vertical velocity. Note that only in the next paragraph we will focus on plumes and slabs by introducing a further criterion based on the excess of temperature. Fig. 6a shows that for the Al-free system the spin state transition modifies the vertical velocity of both upwelling and downwelling material throughout the whole mantle. In particular, the RMS vertical velocity difference for upwelling is 5–15% faster

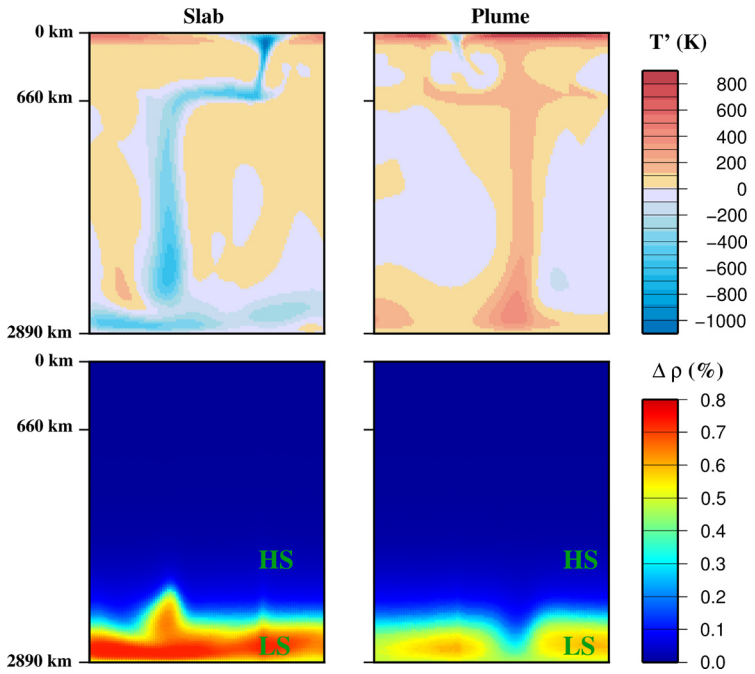

Fig. 4. Vertical cross-section of the anomaly of potential temperature (top) and the density change induced by the spin state transition (bottom) for a typical slab (left) and a typical plume (right). Temperature anomaly is defined as $T - T_m$, where T_m is the average temperature. The density change is equivalent to the spin state: blue is HS state, red is LS state. These results are extracted from the Al-free case. (For interpretation of the references to color in this figure legend, the reader is referred to the web version of this article.)

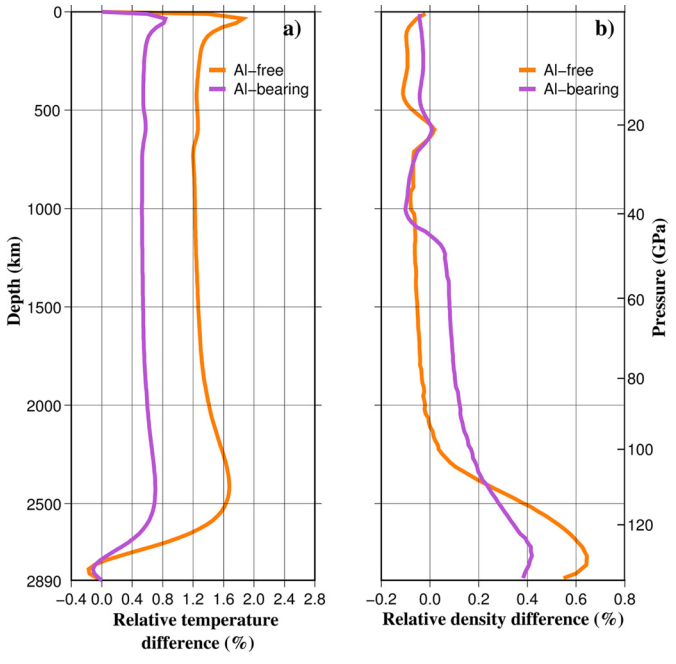

Fig. 5. (a) Horizontally and temporally averaged temperature difference relative to reference (%) for the Al-free case (orange line) and for the Al-bearing case (purple line). (b) A typical relative density difference horizontally averaged (%) for the Al-free case (orange line) and for the Al-bearing case (purple line). The pressure scale is extracted from numerical simulations. (For interpretation of the references to color in this figure legend, the reader is referred to the web version of this article.)

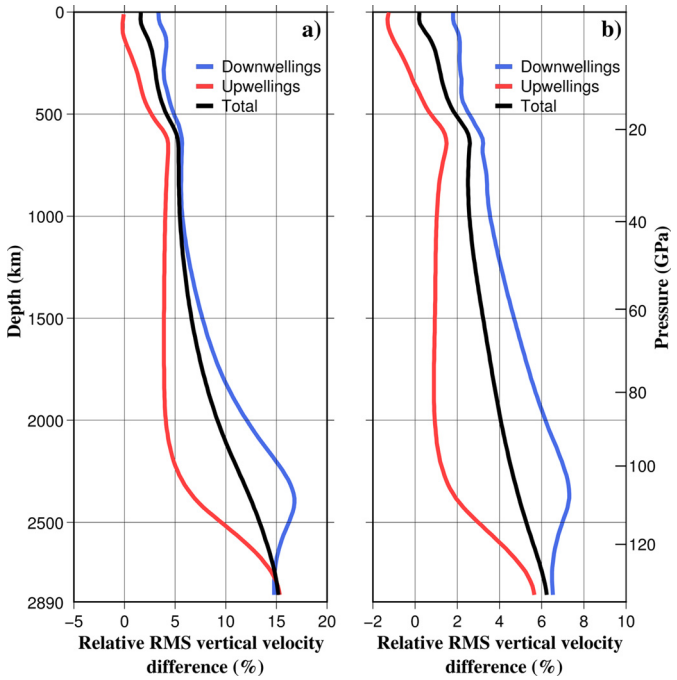

Fig. 6. Horizontally and temporally averaged relative RMS vertical velocity difference (%) versus depth (km). For both Al-free (a) and Al-bearing (b) system, we represent the downwelling velocity (blue lines), the upwelling velocity (red lines), selected as negative or positive flow velocity, respectively, and the velocity of the whole convective fluid (black lines). The pressure scale is extracted from numerical simulations. (For interpretation of the references to color in this figure legend, the reader is referred to the web version of this article.)

in the lowermost mantle (i.e., $D > 2300$ km), it remains constant (∼5% faster) throughout the lower mantle and decreases only in the upper mantle. For downwellings the relative velocity difference is 4–17% faster throughout the lower mantle, reaching a peak value of ∼17% at ∼2400 km. For the sum of the two contributions the relative velocity difference increases with depth, reaching ∼15% at the CMB. For the Al-bearing system (Fig. 6b), the effects of the spin state transition are similar. The main difference bears on the amplitude of the velocity difference, which is less significant for this composition (up to ∼6% for upwellings, up to ∼8% for downwellings and up to ∼6% for the whole convective fluids)

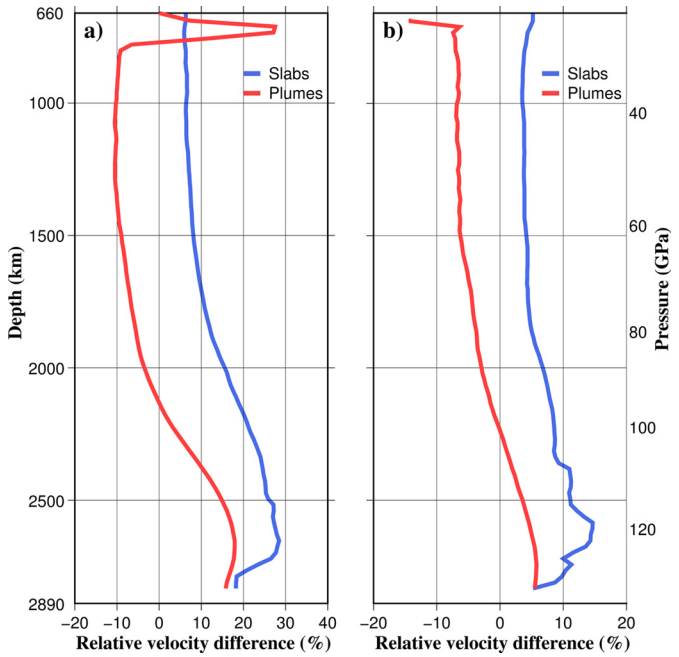

Fig. 7. Horizontally and temporally averaged relative RMS vertical velocity difference (%) versus depth (km). For both Al-free (a) and Al-bearing (b) system, we represent the impact of spin state transition in the lower mantle on slabs (blue lines) and on plumes (red lines), selected via the method explained in the text. The pressure scale is extracted from numerical simulations. (For interpretation of the references to color in this figure legend, the reader is referred to the web version of this article.)

in agreement with the lower density change (Fig. 5b). Surprisingly the relative velocity difference does not seem to be affected by the change of Fe partitioning at 30 GPa.

Note that averages for downwellings and upwellings material, so defined by the vertical velocity, cannot provide detailed information on slabs and plumes, which represent only a small fraction of the whole convective material. To focus on plumes and slabs we need to use a temperature based criterion (Labrosse, 2002). A point (x, y, z) belongs to a plume if:

$$T(x, y, z) > T_{mean}(z) + p_{h,T}[T_{max}(z) - T_{mean}(z)] \tag{18}$$

or to a slab if:

$$T(x, y, z) < T_{mean}(z) + p_{c,T}[T_{min}(z) - T_{mean}(z)], \tag{19}$$

where T_{mean}, T_{min} and T_{max} are the averaged, the minimum and the maximum temperature at a given depth, respectively, $p_{c,T} = p_{h,T} = 0.45$ are constants, the chosen value is from Galsa and Lenkey (2007). We apply this algorithm across all the lower mantle, except for the last 50 km close to the bottom boundary, since slabs do not penetrate the thermal boundary layer. For the Al-free system (Fig. 7a), with the spin state transition plumes are faster (up to 20%) in the lowermost mantle ($D < 2100$ km) but become slower (up to −10%) once they reach shallow depths ($700 < D < 2100$ km), whereas slabs are faster (up to 30%) in the whole lower mantle. For the Al-bearing system (Fig. 7b) the trends are similar, but the relative velocity difference is reduced to ∼15%, showing how important is to include Al in lower mantle composition models. We find that the effect of the spin state transition is to increase slabs and plumes vertical velocities at depths greater than 2100 km (i.e., $P > 100$ GPa). These results show that the simple reasoning presented above, which predicts the vertical velocity solely on the local lateral density difference, is valid at first order but some disagreements remain. For instance plumes and slabs are affected by the spin state transition at the top of the lower mantle, whereas for this pressure–temperature condition there is no lateral density difference. This result is not surprising, since at infinite Prandtl number the whole convective fluid is immediately affected by a local change. Slabs could be faster in the whole mantle because their deepest part, which is undergoing the spin state transition, is able to pull down the whole slab.

We also calculated the averaged time required to travel the lower mantle depth. We found that the spin state transition slightly slows down plumes (2.8% for Al-bearing system and 0.3% for Al-free), but accelerates slabs (8.3% for Al-bearing system and 14.1% for Al-free). Overall, for an Al-free composition, with the spin state transition the RMS vertical velocity is faster in the lower mantle, which implies an enhanced convection. However, the effects of spin state transition on temperature are small compared with our uncertainties. For example the plausible geotherm inferred by Deschamps and Trampert (2004) has an uncertainty of ∼500 K, which is large compared with the 50 K difference caused by the spin state transition. For an Al-bearing composition the amplitude of the relative change of average temperature and velocity is lower and becomes not significant. When we focus on slabs and plumes, rather than study the average vertical flow velocity, we find that the effect of the spin state transition is to enhance their vertical velocity.

5. Discussion

We conducted numerical simulations of mantle convection with and without the density change induced by the spin state transition in Fp. A novel aspect of our approach is to consider that iron content in Fp varies with pressure and temperature, as indicated by recent experiments on iron partition coefficient (K^{Pv-Fp}) between Fp and Pv. Since the experiments show a different behavior of K^{Pv-Fp} depending on alumina content, we explored two end-member mantle compositions, one Al-free (i.e., 75% Pv, 18% Fp, and 7% CaPv) and one Al-bearing, with 4.7 wt% Al_2O_3. The advantage of calculating lower mantle density using experimental measurements of single phase minerals is that we can consider several cases, each with a plausible mantle mineralogy. Our calculated density profiles fit PREM density within 1.5%, and are consistent with recent high temperature experimental data (Komabayashi et al., 2010; Mao et al., 2011). We have shown that for plausible lower mantle compositions, the global density increase of ∼0.7% induced by the spin state transition in Fp has a minor effect on mantle temperature. More precisely, spatially and temporally averaged mantle temperatures differ by less than 50 K between models with and without spin state transition, whereas the total surface heat loss differs by less than 2.5%. For Al-free composition, flow velocity is significantly affected by the spin state transition, since RMS vertical velocity of downwellings and upwellings differ by ∼17% and ∼15%, respectively. However, for Al-bearing composition, the average flow velocity is moderately affected (differ by less than ∼6%).

Bower et al. (2009) found a more important effect of the spin state transition on mantle temperatures (up to 10%) and on the vertical flow velocity (up to 25% while we find up to 15% for Al-free system). There are two reasons for this difference. First, Bower et al. (2009) explored the effect of a 2–4% density increase. This value is appropriate for pure Fp (Lin and Tsuchiya, 2008), but it is certainly excessive for a lower mantle composition with ∼20% Fp. The second reason concerns the range of acceptable values for mantle potential temperature. Petrological studies (e.g., Putirka, 2005 and references therein) indicate that mantle potential temperature is around 1550 K, whereas Bower et al. (2009) geotherm is only at ∼1050 K. The role of the spin state transition is thereby enhanced, since at low temperatures the transition is sharper.

Numerical simulations by Shahnas et al. (2011) include depth dependent properties and consider a plausible lower mantle com-

position. Shahnas et al. (2011) calculate Fp density anomalies caused by the spin state transition, but do not explore different compositions, nor the role of spin driven Fe partitioning. Their density change induced by the spin state transition is relatively high (∼1.8%), if we consider that recent experiments find a 1.5–2% density variation for pure Fp (Mao et al., 2011; Lin et al., 2013). Shahnas et al. (2011) simulations without post-perovskite (PPv) can be compared to our results and indeed show a minor effect on mantle temperature (with a maximum of 3% variation at 1000 km depth) and on the radial mass flux. Only for more extreme models, which reduce to a pure Fp lower mantle, and in presence of the PPv transition, the authors conclude that mantle mixing is enhanced. Shahnas et al. (2011) conclusions are similar to ours, however they did not show the effect on vertical flow velocity, since velocity variations were only inferred from lateral density changes.

In the following we discuss under which conditions it is possible to infer fluid velocity uniquely from local lateral density changes. The simple relation between ascent velocity (V_z) and lateral density change ($\Delta\rho$) was shown by Batchelor (1954) for a steady laminar plume:

$$V_z \propto \frac{r_p^2 \Delta\rho g}{\eta}, \tag{20}$$

where r_p is the plume radius. However, this expression is valid under a number of restrictive conditions: First, it is valid only far from the source and the interfaces; Kaminski and Jaupart (2003) have shown that the velocity is constant only at a distance from the interface corresponding to five times the plume radius. For example, if $r_p = 100$ km, Eq. (20) holds 500 km above the CMB and 500 km below the 660 km discontinuity. Second, it is valid only if the source of buoyant material provides a constant flux over time. Clearly this condition is not satisfied for mantle convection, where time varying plate velocities induce a varying influx at subduction zones. Third, to obtain this constant ascent velocity, we need to make the assumption of zero pressure on the sides of the plume conduit. This implies that the conduit must be straight and continuous, because bending of the conduit induces compression and decompression (Garel et al., 2014). It is clear that mantle plumes and slabs are not straight and continuous. Thus the simple relation between lateral $\Delta\rho$ and vertical flow velocity may have limited applications in the Earth's mantle.

Since the presence of alumina in the lower mantle is widely accepted, the Al-bearing system is the most plausible composition. For this composition, the density change induced by the spin state transition in Fp is small (<0.5%) as well as its impact on dynamics. This is coherent with seismic observations that do not exhibit any mantle layering at the depth range corresponding to the spin state transition. Our results confirm that there is no disagreement between seismic observations and experimental results at high pressure–temperature conditions. The enhanced convection in the lowermost mantle is a robust consequence of the spin state transition, that could affect the stability of the two Large Low Shear Velocity Provinces (LLSVP) beneath Africa and the Pacific (Garnero and McNamara, 2008). The nature of LLSVP is subject of debates, some authors claim a thermal origin (Schuberth et al., 2009; Davies et al., 2012), while most of studies introduce a chemically distinct reservoir (Deschamps and Tackley, 2008, 2009; Li et al., 2014) related to recycled basaltic crust or iron rich primitive material. The significant increase of slabs and plumes velocity in the deepest part of the mantle may imply a destabilization of such reservoirs. However, this suggestion is speculative because of the poor knowledge of the lowermost mantle coupled to the complexity of mantle dynamics.

Finally, we note that we did not explore all the implications of spin state transitions, hence our conclusions could change with the addition of new features. First, we consider only the spin state transition in Fp, whereas spin state transitions also occurs in Pv and in PPv. To the best of our knowledge there is no experimental study at high pressure and temperature for these two minerals, thus it is difficult to build a robust model of spin state transitions. We also choose to not include the PPv in our numerical simulations, unlike Shahnas et al. (2011), because the coexistence of Fp, Pv and PPv with their corresponding Fe partitioning (see Lin et al., 2013; Badro, 2014, and reference therein) would add more complexities. Second, Fe partitioning could have some major consequences on the Earth's mantle, since iron content changes dramatically the radiative thermal conductivity (Goncharov et al., 2010), the electrical conductivity (Dobson and Brodholt, 2000), and may change the viscosity, which is a key parameter for dynamics (Naliboff and Kellogg, 2007). Ammann et al. (2011) find a negligible effect of spin state transitions on viscosity, but the effect of Fe partitioning on viscosity is unknown. Fig. 1 showed that important variations of Fe partitioning are likely to occur in the lower mantle, therefore in a future study we will explore the implications of a viscosity change associated to a Fe partitioning change.

Fe partitioning may also be important to understand yet unexplained observations, for example Ricolleau et al. (2009) highlighted that a typical pyrolitic composition has a density profile with a steeper slope than PREM density; this disagreement cannot be resolved by considering uncertainties of both PREM and experimental results and requires another explanation. Cobden et al. (2009) used mineral physics constraints with their corresponding uncertainties to interpret seismic data. They concluded that the seismic observations can be explained with a superadiabatic geotherm combined to a gradual change of the bulk chemistry. They suggested an increase of the MORB proportion with depth, and they indicated that a Fe-enrichment is also possible. One can speculate that a higher superadiabatic geotherm coupled to an increase of Fe partitioning due to temperature could provide an explanation to seismic observations. Understanding to which extent Fe partitioning affects the lower mantle requires further work and experimental results on effects of temperature, alumina content and bulk iron (Mao et al., 1997; Sakai et al., 2009; Irifune et al., 2010).

Acknowledgements

We thank Rhodri Davies and an anonymous reviewer for their thorough and constructive comments that improved the paper. We also thank John Brodholt for his editorial handling. Numerical computations were performed on the S-CAPAD platform, IPGP, France and using HPC resources from GENCI-IDRIS (Grant 2013-047033). This is IPGP contribution 3612.

Appendix A. Supplementary material

Supplementary material related to this article can be found online at http://dx.doi.org/10.1016/j.epsl.2015.02.009.

References

Ammann, M.W., Brodholt, J.P., Dobson, D.P., 2011. Ferrous iron diffusion in ferropericlase across the spin transition. Earth Planet. Sci. Lett. 302, 393–402. http://dx.doi.org/10.1016/j.epsl.2010.12.031.

Antonangeli, D., Siebert, J., Aracne, C.M., Farber, D.L., Bosak, A., Hoesch, M., Krisch, M., Ryerson, F.J., Fiquet, G., Badro, J., 2011. Spin crossover in ferropericlase at high pressure: a seismologically transparent transition? Science 331, 64–67. http://dx.doi.org/10.1126/science.1198429.

Auzende, A.L., Badro, J., Ryerson, F.J., Weber, P.K., Fallon, S.J., Addad, A., Siebert, J., Fiquet, G., 2008. Element partitioning between magnesium silicate perovskite and ferropericlase: new insights into bulk lower-mantle geochemistry. Earth Planet. Sci. Lett. 269, 164–174. http://dx.doi.org/10.1016/j.epsl.2008.02.001.

Badro, J., 2014. Spin transitions in mantle minerals. Annu. Rev. Earth Planet. Sci. 42, 231–248. http://dx.doi.org/10.1146/annurev-earth-042711-105304.

Badro, J., Fiquet, G., Guyot, F., Rueff, J.P., Struzhkin, V.V., Vankó, G., Monaco, G., 2003. Iron partitioning in Earth's mantle: toward a deep lower mantle discontinuity. Science 300, 789–791. http://dx.doi.org/10.1126/science.1081311.

Badro, J., Rueff, J.P., Vankó, G., Monaco, G., Fiquet, G., Guyot, F., 2004. Electronic transitions in perovskite: possible nonconvecting layers in the lower mantle. Science 305, 383–386. http://dx.doi.org/10.1126/science.1098840.

Badro, J., Fiquet, G., Guyot, F., 2005. Thermochemical State of the Lower Mantle: New Insights from Mineral Physics. Geophysical Monograph Series, vol. 160. AGU, pp. 241–260. http://dx.doi.org/10.1029/160GM15.

Batchelor, G.K., 1954. Heat convection and buoyancy effects in fluids. Q. J. R. Meteorol. Soc. 80, 339–358. http://dx.doi.org/10.1002/qj.49708034504.

Bower, D.J., Gurnis, M., Jackson, J.M., Sturhahn, W., 2009. Enhanced convection and fast plumes in the lower mantle induced by the spin transition in ferropericlase. Geophys. Res. Lett. 36, L10306. http://dx.doi.org/10.1029/2009GL037706.

Brown, J.M., Shankland, T.J., 1981. Thermodynamic parameters in the Earth as determined from seismic profiles. Geophys. J. R. Astron. Soc. 66, 579–596. http://dx.doi.org/10.1111/j.1365-246X.1981.tb04891.x.

Burns, R.G., 1993. Mineralogical Applications of Crystal Field Theory. Cambridge University Press, Cambridge, UK.

Catalli, K., Shim, S.H., Prakapenka, V.B., Zhao, J., Sturhahn, W., Chow, P., Xiao, Y., Liu, H., Cynn, H., Evans, W.J., 2010. Spin state of ferric iron in $MgSiO_3$ perovskite and its effect on elastic properties. Earth Planet. Sci. Lett. 289, 68–75. http://dx.doi.org/10.1016/j.epsl.2009.10.029.

Catalli, K., Shim, S.H., Dera, P., Prakapenka, V.B., Zhao, J., Sturhahn, W., Chow, P., Xiao, Y., Cynn, H., Evans, W.J., 2011. Effects of the Fe^{3+} spin transition on the properties of aluminous perovskite – new insights for lower-mantle seismic heterogeneities. Earth Planet. Sci. Lett. 310, 293–302. http://dx.doi.org/10.1016/j.epsl.2011.08.018.

Cobden, L., Goes, S., Ravenna, M., Styles, E., Cammarano, F., Gallagher, K., Connolly, J.A.D., 2009. Thermochemical interpretation of 1-D seismic data for the lower mantle: the significance of nonadiabatic thermal gradients and compositional heterogeneity. J. Geophys. Res., Solid Earth 114, B11309. http://dx.doi.org/10.1029/2008JB006262.

Cohen, R.E., Mazin, I.I., Isaak, D.G., 1997. Magnetic collapse in transition metal oxides at higher pressure: implications for the Earth. Science 275, 654–657. http://dx.doi.org/10.1126/science.275.5300.654.

Crowhurst, J.C., Brown, J.M., Goncharov, A.F., Jacobsen, S.D., 2008. Elasticity of (Mg, Fe)O through the spin transition of iron in the lower mantle. Science 319, 451–453. http://dx.doi.org/10.1126/science.1149606.

Davies, D.R., Goes, S., Davies, J.H., Schuberth, B.S.A., Bunge, H.P., Ristema, J., 2012. Reconciling dynamic and seismic models of Earths lower mantle: the dominant role of thermal heterogeneity. Earth Planet. Sci. Lett. 353–354, 253–269. http://dx.doi.org/10.1016/j.epsl.2012.08.016.

Deschamps, F., Tackley, P.J., 2008. Searching for models of thermo-chemical convection that explain probabilistic tomography I. Principles and influence of rheological parameters. Phys. Earth Planet. Inter. 171, 357–373. http://dx.doi.org/10.1016/j.pepi.2008.04.016.

Deschamps, F., Tackley, P.J., 2009. Searching for models of thermo-chemical convection that explain probabilistic tomography II – influence of physical and compositional parameters. Phys. Earth Planet. Inter. 176, 1–18. http://dx.doi.org/10.1016/j.pepi.2009.03.012.

Deschamps, F., Trampert, J., 2004. Towards a lower mantle reference temperature and composition. Earth Planet. Sci. Lett. 222, 161–175. http://dx.doi.org/10.1016/j.epsl.2004.02.024.

Dobson, D.P., Brodholt, J.P., 2000. The electrical conductivity of the lower mantle phase magnesiowüstite at high temperatures and pressures. J. Geophys. Res. 105, 531–538. http://dx.doi.org/10.1029/1999JB900242.

Dziewonski, A., Anderson, D.L., 1981. Preliminary earth reference model. Phys. Earth Planet. Inter. 25, 297–356. http://dx.doi.org/10.1016/0031-9201(81)90046-7.

Fei, Y.W., Zhang, L., Corgne, A., Watson, H.C., Ricolleau, A., Meng, Y., Prakapenka, V.B., 2007. Spin transition and equations of state of (Mg,Fe)O solid solutions. Geophys. Res. Lett. 34, L17307. http://dx.doi.org/10.1029/2007GL030712.

Fiquet, G., Dewaele, A., Andrault, D., Kunz, M., Le Bihan, T., 2000. Thermoelastic properties and crystal structure of $MgSiO_3$ perovskite at lower mantle pressure and temperature conditions. Geophys. Res. Lett. 27, 21–24. http://dx.doi.org/10.1029/1999GL008397.

Fyfe, W.S., 1960. The possibility of d-electron uncoupling in olivine at high pressures. Geochim. Cosmochim. Acta 19, 141–143. http://dx.doi.org/10.1016/0016-7037(60)90046-6.

Galsa, A., Lenkey, L., 2007. Quantitative investigation of physical properties of mantle plumes in three-dimensional numerical models. Phys. Fluids 19, 116601. http://dx.doi.org/10.1063/1.2794284.

Garel, F., Goes, S., Davies, D.R., Davies, J.H., Kramer, S.C., Wilson, C.R., 2014. Interactions of subducted slabs with the mantle transition-zone: a regime diagram from 2-D thermo-mechanical models with a mobile trench and an overriding plate. Geochem. Geophys. Geosyst. 15. http://dx.doi.org/10.1002/2014GC005257.

Garnero, E.J., McNamara, A.K., 2008. Structure and dynamics of Earth's lower mantle. Science 320, 626–628. http://dx.doi.org/10.1126/science.1148028.

Goncharov, A.F., Haugen, B.D., Struzhkin, V.V., Beck, P., Jacobsen, S.D., 2008. Radiative thermal conductivity in the Earth's lower mantle. Nature 456, 231–234. http://dx.doi.org/10.1038/nature07412.

Goncharov, A.F., Beck, P., Struzhkin, V.V., Haugen, B.D., Jacobsen, S.D., 2009. Thermal conductivity of lower-mantle minerals. Phys. Earth Planet. Inter. 174, 24–32. http://dx.doi.org/10.1016/j.pepi.2008.07.033.

Goncharov, A.F., Struzhkin, V.V., Montoya, J.A., Kharlamova, S., Kundargi, R., Siebert, J., Badro, J., Antonangeli, D., Ryerson, F.J., Mao, W., 2010. Effects of composition, structure, and spin state on the thermal conductivity of the Earth's lower mantle. Phys. Earth Planet. Inter. 180, 148–153. http://dx.doi.org/10.1016/j.pepi.2010.02.002.

Irifune, T., 1994. Absence of an aluminous phase in the upper part of the Earth's lower mantle. Nature 370, 131–133. http://dx.doi.org/10.1038/370131a0.

Irifune, T., Shinmei, T., McCammon, C.A., Miyajima, N., Rubie, D.C., Frost, D.J., 2010. Iron partitioning and density changes of pyrolite in Earth's lower mantle. Science 327, 193–195. http://dx.doi.org/10.1126/science.1181443.

Jackson, I., 1998. Elasticity, composition and temperature of the Earths lower mantle: a reappraisal. Geophys. J. Int. 134, 291–311. http://dx.doi.org/10.1046/j.1365-246x.1998.00560.x.

Jackson, I., Niesler, H., 1982. The elasticity of periclase to 3 GPa and some geophysical implications. In: High-Pressure Research in Geophysics, pp. 93–113.

Jackson, I., Rigden, S.M., 1996. Analysis of $P-V-T$ data: constraints on the thermoelastic properties of high-pressure minerals. Phys. Earth Planet. Inter. 96, 85–112. http://dx.doi.org/10.1016/0031-9201(96)03143-3.

Jackson, J.M., Sturhahn, W., Shen, G.Y., Zhao, J.Y., Hu, M.Y., Errandonea, D., Bass, J.D., Fei, Y.W., 2005. A synchroton Mössbauer spectroscopy study of $(Mg,Fe)SiO_3$ perovskite up to 120 GPa. Am. Mineral. 90, 199–205. http://dx.doi.org/10.2138/am.2005.1633.

Jackson, J.M., Sinogeikin, S.V., Jacobsen, S.D., Reichmann, H.J., Mackwell, S.J., Bass, J.D., 2006. Single-crystal elasticity and sound velocities of $(Mg_{0.94}Fe_{0.06})O$ ferropericlase to 20 GPa. J. Geophys. Res. 111, B09203. http://dx.doi.org/10.1029/2005JB004052.

Jaupart, C., Labrosse, S., Mareschal, J.C., 2007. Temperatures, Heat and Energy in the Mantle of the Earth. In: Treatise on Geophysics, vol. 7. Elservier, pp. 253–303.

Kaminski, E., Jaupart, C., 2003. Laminar starting plumes in high-Prandtl-number fluids. J. Fluid Mech. 478, 287–298. http://dx.doi.org/10.1017/S0022112002003233.

Kesson, S.E., Fitz Gerald, J.D., Shelley, J.M., 1998. Mineralogy and dynamics of a pyrolite lower mantle. Nature 393, 252–255. http://dx.doi.org/10.1038/30466.

Kobayashi, Y., Kondo, T., Ohtani, E., Hirao, N., Miyajima, N., Yagi, T., Nagase, T., Kikegawa, T., 2005. Fe–Mg partitioning between $(Mg,Fe)SiO_3$ post-perovskite, perovskite, and magnesiowüstite in the Earth's lower mantle. Geophys. Res. Lett. 32, L19301. http://dx.doi.org/10.1029/2005GL023257.

Komabayashi, T., Hirose, K., Nagaya, Y., Sugimura, E., Ohishi, Y., 2010. High-temperature compression of ferropericlase and the effect of temperature on iron spin transition. Earth Planet. Sci. Lett. 297, 691–699. http://dx.doi.org/10.1016/j.epsl.2010.07.025.

Labrosse, S., 2002. Hotspots, mantle plumes and core heat loss. Earth Planet. Sci. Lett. 199, 147–156. http://dx.doi.org/10.1016/S0012-821X(02)00537-X.

Li, J., Struzhkin, V.V., Mao, H.K., Shu, J., Hemley, R.J., Fei, Y., Mysen, B., Dera, P., Prakapenka, V., Shen, G., 2004. Electronic spin state of iron in lower mantle perovskite. Proc. Natl. Acad. Sci. USA 101, 14027–14030. http://dx.doi.org/10.1073/pnas.0405804101.

Li, Y., Deschamps, F., Tackley, P.J., 2014. The stability and structure of primordial reservoirs in the lower mantle: insights from models of thermochemical convection in three-dimensional spherical geometry. Geophys. J. Int. 199, 914–930. http://dx.doi.org/10.1093/gji/ggu295.

Lin, J.F., Tsuchiya, T., 2008. Spin transition of iron in the Earth's lower mantle. Phys. Earth Planet. Inter. 170, 248–259. http://dx.doi.org/10.1016/j.pepi.2008.01.005.

Lin, J.F., Jacobsen, S.D., Sturhahn, W., Jackson, J.M., Zhao, J., Yoo, C.S., 2006. Sound velocities of ferropericlase in the Earth's lower mantle. Geophys. Res. Lett. 33, L22304. http://dx.doi.org/10.1029/2006GL028099.

Lin, J.F., Vankó, G., Jacobsen, S.D., Iota, V., Struzhkin, V.V., Prakapenka, V.B., Kuznetsov, A., Yoo, C.S., 2007a. Spin transition zone in Earth's lower mantle. Science 317, 1740–1743. http://dx.doi.org/10.1126/science.1144997.

Lin, J.F., Weir, S.T., Jackson, D.D., Evans, W.J., Vohra, Y.K., Qiu, W., Yoo, C.S., 2007b. Electrical conductivity of the lower-mantle ferropericlase across the electronic spin transition. Geophys. Res. Lett. 34, L16305. http://dx.doi.org/10.1029/2007GL030523.

Lin, J.F., Speziale, S., Mao, Z., Marquardt, H., 2013. Effects of the electronic spin transitions of iron in lower mantle minerals: implications for deep mantle geophysics and geochemistry. Rev. Geophys. 51, 244–275. http://dx.doi.org/10.1002/rog.20010.

Lundin, S., Catalli, K., Santillán, J., Shim, S.H., Prakapenka, V.B., Kunz, M., Meng, Y., 2008. Effect of Fe on the equation of state of mantle silicate perovskite over 1 Mbar. Phys. Earth Planet. Inter. 168, 97–102. http://dx.doi.org/10.1016/j.pepi.2008.05.002.

Mao, H.K., Shen, G., Hemley, R.J., 1997. Multivariable dependence of Fe–Mg partitioning in the lower mantle. Science 278, 2098–2100. http://dx.doi.org/10.1126/science.278.5346.2098.

Mao, Z., Lin, J.F., Liu, J., Prakapenka, V.B., 2011. Thermal equation of state of lower-mantle ferropericlase across the spin crossover. Geophys. Res. Lett. 38, L23308. http://dx.doi.org/10.1029/2011GL049915.

Murakami, M., Hirose, K., Sata, N., Ohishi, Y., 2005. Post-perovskite phase transition and mineral chemistry in the pyrolitic lowermost mantle. Geophys. Res. Lett. 32, L03304. http://dx.doi.org/10.1029/2004GL021956.

Murakami, M., Ohishi, Y., Hirao, N., Hirose, K., 2012. A perovskitic lower mantle inferred from high-pressure, high-temperature sound velocity data. Nature 485, 90–94. http://dx.doi.org/10.1038/nature11004.

Naliboff, J.B., Kellogg, L.H., 2007. Can large increases in viscosity and thermal conductivity preserve large-scale heterogeneity in the mantle? Phys. Earth Planet. Inter. 161, 86–102. http://dx.doi.org/10.1016/j.pepi.2007.01.009.

Navrotsky, A., 1999. A lesson from ceramics. Science 284, 1788–1789. http://dx.doi.org/10.1126/science.284.5421.1788.

Putirka, K.D., 2005. Mantle potential temperatures at Hawaii, Iceland, and the mid-ocean ridge system, as inferred from olivine phenocrysts: evidence for thermally driven mantle plumes. Geochem. Geophys. Geosyst. 6, Q05L08. http://dx.doi.org/10.1029/2005GC000915.

Ricolleau, A., Fei, Y., Cottrell, E., Watson, H., Deng, L., Zhang, L., Fiquet, G., Auzende, A.L., Roskosz, M., Morard, G., Prakapenka, V.B., 2009. Density profile of pyrolite under the lower mantle conditions. Geophys. Res. Lett. 36, L06302. http://dx.doi.org/10.1029/2008GL036759.

Ringwood, A.E., 1982. Phase transformations and differentiation in subducted lithosphere: implications for mantle dynamics basalt petrogenesis and crustal evolution. J. Geol. 90, 611–643. http://dx.doi.org/10.1086/628721.

Sakai, T., Ohtani, E., Terasaki, H., Sawada, N., Kobayashi, Y., Miyahara, M., Nishijima, M., Hirao, N., Ohishi, Y., Kikegawa, T., 2009. Fe–Mg partitioning between perovskite and ferropericlase in the lower mantle. Am. Mineral. 94, 921–925. http://dx.doi.org/10.2138/am.2009.3123.

Schuberth, B.S.A., Bunge, H.P., Ristema, J., 2009. Tomographic filtering of high-resolution mantle circulation models: can seismic heterogeneity be explained by temperature alone? Geochem. Geophys. Geosyst. 10. http://dx.doi.org/10.1029/2009GC002401.

Shahnas, M.H., Peltier, W.R., Wu, Z., Wentzcovitch, R., 2011. The high-pressure electronic spin transition in iron: potential impacts upon mantle mixing. J. Geophys. Res. 116, B08205. http://dx.doi.org/10.1029/2010JB007965.

Sherman, D.M., 1988. High-spin to low-spin transition of iron (II) oxides at high pressures: possible effects on the physics and chemistry of the lower mantle. In: Adv. Phys. Geochem., vol. 7. Springer, New York.

Shim, S.H., Duffy, T.S., Shen, G., 2000a. The equation of state of $CaSiO_3$ perovskite to 108 GPa at 300 K. Phys. Earth Planet. Inter. 120, 327–338. http://dx.doi.org/10.1016/S0031-9201(00)00154-0.

Shim, S.H., Duffy, T.S., Shen, G., 2000b. The stability and PVT equation of state of $CaSiO_3$ perovskite in the Earth's lower mantle. J. Geophys. Res. 105, 25955–25968. http://dx.doi.org/10.1029/2000JB900183.

Sinmyo, R., Hirose, K., 2013. Iron partitioning in pyrolitic lower mantle. Phys. Chem. Miner. 40, 107–113. http://dx.doi.org/10.1007/s00269-012-0551-7.

Sinmyo, R., Hirose, K., Nishio-Hamane, D., Seto, Y., Fujino, K., Sata, N., Ohishi, Y., 2008. Partitioning of iron between perovskite/postperovskite and ferropericlase in the lower mantle. J. Geophys. Res. 113, B11204. http://dx.doi.org/10.1029/2008JB005730.

Speziale, S., Zha, C.S., Duffy, T.S., Hemley, R.J., Mao, H.K., 2001. Quasi-hydrostatic compression of magnesium oxide to 52 GPa: implications for the pressure–volume–temperature equation of state. J. Geophys. Res. 106, 515–528. http://dx.doi.org/10.1029/2000JB900318.

Sturhahn, W., Jackson, J.M., Lin, J.F., 2005. The spin state of iron in minerals of Earth's lower mantle. Geophys. Res. Lett. 32, L12307. http://dx.doi.org/10.1029/2005GL022802.

Tackley, P.J., 1996. Effects of strongly variable viscosity on three-dimensional compressible convection in planetary mantles. J. Geophys. Res. 101, 3311–3332. http://dx.doi.org/10.1029/95JB03211.

Tsuchiya, T., Wentzcovitch, R.M., da Silva, C.R.S., de Gironcoli, S., 2006. Spin transition in magnesiowstite in Earth's lower mantle. Phys. Rev. Lett. 96, 198501. http://dx.doi.org/10.1103/PhysRevLett.96.198501.

Wood, B.J., 2000. Phase transformations and partitioning relations in peridotite under lower mantle conditions. Earth Planet. Sci. Lett. 174, 341–354. http://dx.doi.org/10.1016/S0012-821X(99)00273-3.